

Multi-Agent DRL for V2X Resource Allocation: Disentangling Challenges and Benchmarking Solutions

Siyuan Wang¹, Lei Lei¹, *Senior Member, IEEE*, Pranav Maheshwari¹, Sam Bellefeuille¹, Kan Zheng² *Fellow, IEEE*, Dusit Niyato³, *Fellow, IEEE*

Abstract—Multi-agent deep reinforcement learning (DRL) has emerged as a promising approach for radio resource allocation (RRA) in cellular vehicle-to-everything (C-V2X) networks. However, the multifaceted challenges inherent to multi-agent reinforcement learning (MARL)—including non-stationarity, coordination difficulty, large action spaces, partial observability, and limited robustness and generalization—are often intertwined, making it difficult to understand their individual impact on performance in vehicular environments. Moreover, existing studies typically rely on different baseline MARL algorithms, and a systematic comparison of their capabilities in addressing specific challenges in C-V2X RRA remains lacking. In this paper, we bridge this gap by formulating C-V2X RRA as a sequence of multi-agent interference games with progressively increasing complexity, each designed to isolate a key MARL challenge. Based on these formulations, we construct a suite of learning tasks that enable controlled evaluation of performance degradation attributable to each challenge. We further develop large-scale, diverse training and testing datasets using SUMO-generated highway traces to capture a wide range of vehicular topologies and corresponding interference patterns. Through extensive benchmarking of representative MARL algorithms, we identify policy robustness and generalization across diverse vehicular topologies as the dominant challenge in C-V2X RRA. We further show that, on the most challenging task, the best-performing actor-critic method outperforms the best-performing value-based approach by 42%. By emphasizing the need for zero-shot policy transfer to both seen and unseen topologies at runtime, and by open-sourcing the code, datasets, and interference-game benchmark suite, this work provides a systematic and reproducible foundation for evaluating and advancing MARL algorithms in vehicular networks.

Index Terms—Deep Reinforcement Learning; V2X; Radio Resource Allocation, MARL

I. INTRODUCTION

Cellular Vehicle-to-Everything (C-V2X) is a critical technology in the evolution of intelligent transportation sys-

An earlier version of this work appeared at the IEEE International Conference on Communications (ICC) 2025 [1]. This version extends the prior work by enlarging and systematizing the training and testing datasets with open-source dataset and code to enable representative and reproducible evaluations, expanding the scalability analysis to more agents, and providing deeper experimental analysis, an expanded literature review, and key insights into future work.

¹S. Wang, L. Lei, P. Maheshwari, and S. Bellefeuille are with the College of Engineering, University of Guelph, Guelph, Ontario, Canada (e-mail: leil@uoguelph.ca).

²K. Zheng is with the College of Electrical Engineering and Computer Sciences, Ningbo University, Ningbo, 315211, China.

³D. Niyato is with the College of Computing and Data Science, Nanyang Technological University, 50 Nanyang Avenue, Singapore 639798.

tems, enabling vehicle-to-vehicle (V2V) and vehicle-to-infrastructure (V2I) communications. Radio Resource Allocation (RRA), which manages communication resources such as spectrum and power among multiple vehicles and infrastructure nodes, plays a key role in the performance of C-V2X networks [2].

In recent years, Deep Reinforcement Learning (DRL) has emerged as a powerful tool for addressing the complexities of RRA in C-V2X networks. Unlike traditional optimization methods that often rely on predefined models, DRL leverages deep neural networks (DNNs) to learn optimal policies directly from interaction data [3]. This data-driven approach allows DRL to adapt to the dynamic and uncertain nature of vehicular environments, making it particularly well-suited for real-time decision-making tasks in RRA [4].

RRA in C-V2X networks is inherently a multi-agent problem, as efficient resource sharing depends on the coordinated actions of multiple vehicles and devices. This multi-agent aspect has led to the exploration of Multi-Agent Reinforcement Learning (MARL) techniques [5], which extend the principles of Reinforcement Learning (RL) to scenarios where multiple agents interact within a shared environment.

Recent research has highlighted the potential of MARL in C-V2X networks [4], [6]. A growing body of work has explored key MARL challenges and proposed promising solutions [7]–[13]. While these studies have provided valuable contributions, several critical issues remain insufficiently addressed, which this paper aims to tackle.

- MARL faces several challenges, including non-stationarity, coordination difficulty, large action spaces, partial observability, and the need for robustness and generalization [14]. The impact of these challenges can vary significantly across environments, as issues that are minor in one setting may become critical in another [15]. Understanding how each challenge affects C-V2X RRA performance is therefore essential for guiding future research. Achieving this understanding requires a systematic methodology that can isolate individual MARL challenges and evaluate algorithm performance in carefully designed environments, both with and without each challenge.
- In recent years, a range of classical MARL algorithms has been developed in the machine learning (ML) community [14]. In the C-V2X domain, existing studies have typically adopted one or more of these algorithms, or

used them as building blocks for more advanced methods, to tackle the RRA problem. However, a significant gap remains in systematically evaluating and comparing these classical multi-agent DRL algorithms within C-V2X environments—particularly regarding their ability to address specific MARL challenges—which is crucial for guiding algorithm selection for RRA tasks. Although [15] provides a comprehensive benchmark of common multi-agent DRL algorithms across various gaming environments, these results do not directly translate to C-V2X scenarios due to fundamental differences in system dynamics and performance objectives.

To address the research gaps outlined above, the main contributions of this work are summarized as follows.

- We formulate RRA problems in C-V2X networks as a series of multi-agent interference games with ascending complexity, as more realistic factors are incorporated. We analyze the MARL challenges for each game, noting that the challenges from simpler games persist in the more complex ones, with additional challenges arising as complexity increases.
- Based on these interference games, we design learning tasks that isolate individual MARL challenges and benchmark eight classical multi-agent DRL algorithms across these tasks, assessing their ability to address different MARL challenges. Vehicle position datasets are generated using the SUMO simulator to capture diverse interference conditions.
- From our results, we identify learning policies that are robust to diverse vehicular topologies and generalize to unseen ones as the most critical MARL challenge for C-V2X RRA tasks. Actor-critic algorithms outperform value-based ones in complex tasks with diverse topologies. For the best-performing PPO algorithm [16], Centralized Training with Decentralized Execution (CTDE) offers minor improvement over independent learning (IL). Consequently, Independent PPO (IPPO) is recommended as a baseline for its balance of performance and scalability. Our study also highlights the need for zero-shot policy transfer across topologies.
- By open-sourcing our code, datasets, and benchmark suite¹, we provide a systematic, reproducible foundation for evaluating and advancing MARL algorithms in vehicular networks.

The remainder of the paper is organized as follows. Section II reviews related work. Section III describes the C-V2X communication system model. Section IV formulates the RRA problem as a series of multi-agent interference games. Section V introduces the eight MARL algorithms evaluated in this study. Section VI details the experimental setup, while the results and discussion were presented in Section VII. Finally, Section VIII concludes the paper.

II. RELATED WORKS

The application of MARL to RRA in C-V2X communications has been extensively investigated in recent years. In

this section, we review and compare relevant studies from two perspectives—the employed DRL algorithms and the characteristics of the C-V2X environment—as summarized in Table I.

A. DRL Algorithms

DRL algorithms can be broadly categorized into value-based, policy gradient, and actor–critic methods [26]. In multi-agent settings, two commonly used learning frameworks are IL and CTDE. In C-V2X RRA, value-based IL approaches have been the most widely explored [4], [6]–[11], [17], [18].

Early work in this domain applied deep Q networks (DQN) independently at each agent for decentralized RRA, demonstrating performance gains over traditional methods [4]. Subsequent studies introduced various enhancements to mitigate IL challenges, including multi-agent fingerprints [6] and hysteretic Q-learning with concurrent experience replay trajectory (CERT) [7] to tackle non-stationarity, as well as emergent inter-agent communication [8] and attention-based observation construction [9] to address partial observability. To improve scalability, mean-field approximations combined with Nash Q-learning were explored in large-scale networks [10]. Several works adopted Double DQN (DDQN) to reduce overestimation bias [17], [18], with additional action sharing for coordination in [18]. Graph neural networks were further integrated with DDQN to extract compact representations from local observations and mitigate partial observability [11]. In contrast, value-based CTDE methods remain relatively under-explored for C-V2X RRA; a representative example is [19], which employs QMIX for coordinated decision-making.

Beyond value-based methods, policy gradient and actor–critic methods have also been explored in recent works. A vanilla policy-gradient IL method is adopted within a federated learning framework in [20]. In contrast, actor–critic algorithms have been more widely adopted. PPO is independently deployed by each agent in [21], while CTDE is combined with PPO for coordinated RRA in multi-platoon and general settings [22], [23]. Multi-agent deep deterministic policy gradient (MADDPG) [27], the CTDE extension of DDPG [28], is applied to platoon-based and semantic-aware C-V2X RRA in [24], [25]. Hybrid designs have also been explored, such as combining DQN and DDPG with meta-DRL to accelerate adaptation in dynamic environments [12].

B. C-V2X Environment

1) *Urban vs. Highway Scenarios*: Most C-V2X evaluation studies adopt the road-traffic scenarios defined in 3GPP TR 36.885 [29], which specifies the UE distribution and mobility model, channel model, and traffic model for two primary environments: an urban scenario and a highway scenario. In the existing literature, urban scenarios are extensively studied [4], [7], [9]–[12], [17]–[20], [25], while highway scenarios have received less attention [12], [23].

2) *Number of V2V and V2I links*: Most C-V2X studies adopt a framework where each V2I link is assigned a dedicated uplink subchannel, while V2V links share these subchannels through spectrum reuse [4], [6]. Thus, the number of V2V

¹<https://github.com/Deepinlab2023/V2X-MARL-Bench>

TABLE I: Literature Review of MARL Applications in C-V2X Environments

Reference	Scenario	# V2V	# V2I	Speed	Payload	DRL Algorithm
[4]	Urban	60-300	-	36 km/h	Train: - Test: -	DQN
[6]	Urban	4	4	36 km/h	Train: $2 \times 1060\text{B}$ Test: $(1, \dots, 6) \times 1060\text{B}$	DQN (fingerprint)
[7]	Urban	4/8	4/8	36–54 km/h	Train: $6 \times 1060\text{B}$ Test: $(1, \dots, 6) \times 1060\text{B}$	Hysteretic D3RQN
[8]	Urban	4	4	36/54 km/h	Train: $(1, \dots, 6) \times 210\text{B}$ Test: $(1, \dots, 6) \times 210\text{B}$	DQN (emergent comm.)
[9]	Urban	4	4	36–54 km/h	Train: $2 \times 1060\text{B}$ Test: $(1, \dots, 6) \times 1060\text{B}$	DQN (attention)
[10]	Urban	8-32	-	36–144 km/h	Train: - Test: $2 \times 1060\text{B}$	DQN (mean-field)
[17]	Urban	4	4	10–60 km/h	Train: $n \times 1060\text{B}$ Test: $n \times 1060\text{B}$	DDQN
[18]	Urban	5-25	3-12	-	Train: - Test: -	DDQN (federated)
[11]	Urban	60-300	-	-	Train: - Test: -	DDQN (GNN)
[19]	Urban	4	4	36 km/h	Train: $(1, \dots, 6) \times 1060\text{B}$ Test: $(1, \dots, 6) \times 1060\text{B}$	QMIX
[20]	Urban	4-24	4-8	36–54 km/h	Train: $2 \times 1060\text{B}$ Test: $(1, \dots, 6) \times 1060\text{B}$	policy gradient (federated)
[21]	Urban	0	5	36 km/h	Train: - Test: -	MAPPO
[22]	Highway (platooning)	-	25	10–90 km/h	Train: 300B Test: 300B	MAPPO
[23]	Highway	48	3	-	Train: 300–12000B Test: 300–12000B	IPPO
[24]	Urban (platooning)	15-45	5-7	36–54 km/h	Train: 4000B Test: 4000B	MADDPG
[25]	Urban (platooning)	16	4	36 km/h	Train: - Test: -	MADDPG
[12]	Urban / Highway	4-20	4	50-108 km/h	Train: $1 \times 1060\text{B}$ Test: $(1, \dots, 6) \times 1060\text{B}$	DQN + DDPG

“-” indicates that the parameter value is not specified in the experiments.

links corresponds to the number of agents, and the number of V2I links corresponds to the number of subchannels. The most common configuration includes four V2I and four V2V links [6], [7], [9], [17], [19]. Some studies consider larger networks with up to 10–32 V2V links [7], [10], [12], [18], [20], or even 300 V2V links divided into batches [4], [11].

3) *Vehicle Speed and Density*: Although 3GPP TR 36.885 [29] and ETSI TR 103 766 [30] specify vehicle speeds, densities, and speed–density relationships for reproducible C-V2X evaluations, existing literature generally does not follow these values strictly. 3GPP TR 36.885 defines target vehicle speeds of 15 km/h and 60 km/h for urban scenarios and 140 km/h and 70 km/h for highway scenarios, with vehicle density determined by a 2.5-second headway rule. ETSI TR 103 766 further provides six highway speed–density configurations, ranging from high-speed cases (250 km/h at 35 veh/km) to congested conditions (50 km/h at 500 veh/km) [30]. However, most existing studies use vehicle speeds in the range of 36–54 km/h [4], [6]–[9], [19]–[21], [24], [25], and vehicle density is often left unspecified. Since vehicle density strongly influences V2V interference, this absence poses challenges for cross-study comparison.

4) *Payload Sizes*: Most existing works use payload sizes that are integer multiples (1–6) of 1,060 bytes [7], [9], [10], [12], [17], [19], [20]. Typically, the payload size is fixed during training and varied during testing to examine generalization. An agent trained on a large payload (e.g., $6 \times 1,060$ bytes) can readily handle smaller payloads, but the reverse does not necessarily hold. In summary, the lack of standardized

evaluation settings across studies highlights the need for a unified benchmarking framework.

III. C-V2X COMMUNICATION SYSTEM

We consider a typical C-V2X network, where V2V links coexist with V2I links [29]. A V2I link connects a vehicle to the BS and can be used for high-throughput services. A V2V link connects a pair of neighboring vehicles for periodic transmission of cooperative awareness messages (CAM) to support advanced driving services.

In order to enhance spectrum utilization, we consider that L V2V links share the uplink resources orthogonally allocated to M V2I links. Without loss of generality, we assume that every V2I link $m \in \mathcal{M} = \{0, \dots, M-1\}$ is pre-assigned subchannel m with constant transmit power P_m^I [6]. Moreover, one or more V2V links $i \in \mathcal{L} = \{0, \dots, L-1\}$ can reuse the subchannels of the V2I links for CAM transmission.

The time is discretized into equal-length control intervals, indexed by $k \in \mathcal{K} = \{0, 1, \dots\}$. At the beginning of each control interval k (i.e., time kT), the driving status of the transmitting vehicle of each V2V link i (i.e., V2V transmitter i) samples its driving status to form the CAM and buffers it in a queue before transmitting the data to the corresponding receiving vehicle (i.e., V2V receiver i).

Each control interval k is further divided into T communication intervals indexed by $t \in \mathcal{T} = \{0, 1, \dots, T-1\}$ on a faster timescale. Each communication interval has a length of Δt ms corresponding to the subframe duration in C-V2X communications. We consider dynamic scheduling [13],

where the V2V transmitters make RRA decisions at time $kT + t$, $k \in \mathcal{K}$, $t \in \mathcal{T}$, and the corresponding communication interval is represented as (k, t) . In the rest of the paper, we will use $x_{(k,t)} := x((kT + t)\Delta t)$ to represent any variable x at the beginning of communication interval (k, t) .

We use the binary allocation indicator $\theta_{i,m,(k,t)} \in \{0, 1\}$ to indicate whether V2V link i occupies subchannel m at communication interval (k, t) or not. Moreover, we consider that each V2V link i occupies at most one subchannel, i.e., $\sum_{m=0}^{M-1} \theta_{i,m,(k,t)} \leq 1$.

1) *Channel Gain*: The instantaneous channel gain of V2V link i over subchannel m (occupied by V2I link m) at communication interval (k, t) is denoted by $G_{i,m,(k,t)}$. $G_{i,m,(k,t)}$ remains constant within a communication interval, and can be written as

$$G_{i,m,(k,t)} = \alpha_{i,(k,t)} h_{i,m,(k,t)}, \quad (1)$$

where $\alpha_{i,(k,t)}$ captures the large-scale fading effects including path loss and shadowing, which are assumed to be frequency independent. $h_{i,m,(k,t)}$ corresponds to small-scale fading, which can be regarded as identically distributed random variables with unit mean on all subchannels. We consider that $G_{i,m,(k,t)}$ is a Markov process [31], where the probability of $G_{i,m,(k,t)}$ taking a specific value only depends on the value of $G_{i,m,(k,t-1)}$.

Similarly, let $G_{m,(k,t)}$ denote the channel gain of the V2I link m ; $G_{i,B,m,(k,t)}$ denote the interference channel gain from V2V link i transmitter to V2I link m receiver; $G_{B,i,m,(k,t)}$ represent the interference channel gain from V2I link m transmitter to V2V link i receiver; and $G_{j,i,m,(k,t)}$ be the interference channel gain from the V2V link j transmitter to the V2V link i receiver over the subchannel m .

2) *Signal-to-Interference-plus-Noise Ratio (SINR)*: The SINR $\gamma_{m,(k,t)}$ and $\gamma_{i,m,(k,t)}$ of V2I link m and V2V link i on subchannel m at communication interval (k, t) are derived by

$$\gamma_{m,(k,t)} = \frac{P_m^I G_{m,(k,t)}}{\sigma^2 + \sum_{i \in \mathcal{L}} \theta_{i,m,(k,t)} P_{i,m,(k,t)}^V G_{i,B,m,(k,t)}}, \quad (2)$$

and

$$\gamma_{i,m,(k,t)} = \frac{P_{i,m,(k,t)}^V G_{i,m,(k,t)}}{\sigma^2 + I_{i,m,(k,t)}}, \quad (3)$$

respectively, where $P_{i,m,(k,t)}^V$ is the transmit power of V2V link i over the subchannel m at communication interval (k, t) . σ^2 is the power of channel noise which satisfies the independent Gaussian distribution with a zero mean value. $I_{i,m,(k,t)}$ is the total interference power received by V2V link i over subchannel m , where

$$I_{i,m,(k,t)} = P_m^I G_{B,i,m,(k,t)} + \sum_{j \in \mathcal{L} \setminus \{i\}} \theta_{j,m,(k,t)} P_{j,m,(k,t)}^V G_{j,i,m,(k,t)}.$$

We discretize the transmit power $P_{i,m,(k,t)}^V$ to four levels for ease of learning and practical circuit restriction [6], [7], i.e., $P_{i,m,(k,t)}^V \in \mathcal{A}_P = \{23, 15, 5, -100\}$ dBm. Note that -100 dBm can be considered as zero transmit power.

3) *Instantaneous Data Rate*: The instantaneous data rates $r_{m,(k,t)}$ and $r_{i,(k,t)}$ of V2I link m and V2V link i at communication interval (k, t) are respectively derived as

$$r_{m,(k,t)} = W \log_2(1 + \gamma_{m,(k,t)}), \quad (4)$$

and

$$r_{i,(k,t)} = \sum_{m=0}^{M-1} \theta_{i,m,(k,t)} W \log_2(1 + \gamma_{i,m,(k,t)}), \quad (5)$$

where W is the bandwidth of a subchannel.

Let $r_{i,(k,t)}^{\text{CAM}}$ denote the transmission rate of V2V link i in terms of CAM at communication interval (k, t) , which is given by

$$r_{i,(k,t)}^{\text{CAM}} = \frac{r_{i,(k,t)}}{N_c}, \quad (6)$$

where N_c is the constant CAM size.

4) *Queuing Dynamic*: Each V2V transmitter $i \in \mathcal{L}$ has a buffer to store its CAM. Let $q_{i,(k,t)}^{\text{CAM}}$ denote the queue length of V2V transmitter i , in number of CAMs, at communication interval (k, t) . At the beginning of the first communication interval $(k, 0)$ of each control interval $k \in \mathcal{K}$, V2V transmitter i samples the driving status and generates a new CAM, which replaces any CAMs left undelivered from the previous control interval. Therefore, the queue length at the start of each control interval is set to $q_{i,(k,0)}^{\text{CAM}} = 1$ [13].

At each communication interval (k, t) , $t \in \mathcal{T}$, within control interval k , the queue length decreases according to the number of CAMs transmitted, with the constraint that it cannot become negative: $q_{i,(k,t+1)}^{\text{CAM}} = \max[0, q_{i,(k,t)}^{\text{CAM}} - r_{i,(k,t)}^{\text{CAM}} \Delta t]$.

To capture the discontinuity at control interval boundaries, we denote by $q_{i,(k,T)}^{\text{CAM}}$ the queue length at the end of the last communication interval $(k, T-1)$ of control interval k . Note that $q_{i,(k,T)}^{\text{CAM}} \neq q_{i,(k+1,0)}^{\text{CAM}}$ because the queue is reset at the start of each new control interval.

The queue process thus evolves as

$$q_{i,(k,t+1)}^{\text{CAM}} = \begin{cases} 1, & \text{if } t = 0 \\ \max[0, q_{i,(k,t)}^{\text{CAM}} - r_{i,(k,t)}^{\text{CAM}} \Delta t], & \text{otherwise} \end{cases}. \quad (7)$$

IV. C-V2X MULTI-AGENT ENVIRONMENT

In this section, we formulate of the RRA problem in C-V2X as a series of multi-agent interference games. Each successive game builds upon the previous one and captures more realistic factors, resulting in increasing complexity.

A. Normal-Form Interference Game (NFIG)

1) *Environment model*: Without loss of generality, we consider a snapshot of the channel gains at the communication interval (k, t) is captured. The objective is to derive the optimal policy that prescribes the subchannel allocation $\{\theta_{i,m,(k,t)}\}_{m \in \mathcal{M}}$ and transmit power $\{P_{i,m,(k,t)}^V\}_{m \in \mathcal{M}}$ for each V2V link i , so that the sum data rate of all the V2V and V2I links is maximized for this specific communication interval. This simple problem can be formulated as a normal-form game consisting of

- Finite set of V2V agents \mathcal{L} ;
- For each agent $i \in \mathcal{L}$:
 - action $a_i = \{\theta_{i,m}, P_{i,m}^V\}_{m \in \mathcal{M}}$;
 - common reward

$$R = \lambda_1 \sum_{m \in \mathcal{M}} r_{m,(k,t)} + \lambda_2 \sum_{i \in \mathcal{L}} r_{i,(k,t)}, \quad (8)$$

where λ_1 and λ_2 are weighting coefficients reflecting the relative importance of V2I and V2V objectives, respectively.

Since the normal-form game defines a single interaction between the agents and environment, i.e., the time horizon is 1, the communication interval index (k, t) is omitted in the above notations. Each agent i samples an action a_i with probability $\pi_i(a_i)$ given by its policy. The actions of all the agents form a joint action $a = \{a_i\}_{i \in \mathcal{L}}$. Finally, each agent receives the common reward based on the reward function and the joint action.

2) *MARL challenges*: The main challenges faced by MARL algorithms in the NFIG environment stem from the lack of awareness of other agents' actions or policies, making coordination difficult. As all agents initially explore actions randomly, an agent may be penalized due to poor decisions made by other agents, even if it has chosen the optimal action. If the penalties for miscoordination are high, the agent is likely to favor a 'safe' action that ensures an acceptable reward regardless of the actions of others. Specifically, this issue leads to two primary types of pathologies [32], as described below.

- *Relative overgeneralization*: A suboptimal Nash Equilibrium in the joint action space is preferred over an optimal Nash Equilibrium because each agent's action in the suboptimal equilibrium appears more favorable when other agents choose actions randomly.
- *Miscoordination*: When multiple optimal Nash Equilibria exist, one agent may choose an action corresponding to one equilibrium, while another agent selects an action corresponding to a different equilibrium, leading to poor joint actions.

Another well-known challenge is the *non-stationary environment* caused by agents' evolving policies during learning, which leads to the fluctuating values of agents' actions over time and makes it difficult to achieve convergence.

B. Stochastic Interference Game (SIG)

1) *Environment model*: Consider the more practical case when the instantaneous data rate of the V2V links and V2I links vary over time due to the changing distances between the transmitters and receivers and the fast fading effects. The optimization objective is to maximize the V2I throughput as well as the probability of fully delivering the newly generated CAM within each control interval. This problem can be formulated as a stochastic game consisting of

- State $s_{(k,t)} = (G_{(k,t)}, q_{(k,t)}^{\text{CAM}}, t)$, where $G_{(k,t)} = \{\{G_{i,m,(k,t)}\}_{i \in \mathcal{L}}, \{G_{j,i,m,(k,t)}\}_{i,j \in \mathcal{L}}, \{G_{B,i,m,(k,t)}\}_{i \in \mathcal{L}}, \{G_{i,B,m,(k,t)}\}_{i \in \mathcal{L}}, G_{m,(k,t)}\}_{m \in \mathcal{M}}$, and $q_{(k,t)}^{\text{CAM}} = \{q_{i,(k,t)}^{\text{CAM}}\}_{i \in \mathcal{L}}$. The state is thus composed of the channel gains of all the V2V links, V2I links, and interference

links on all the subchannels, as well as the queue length of all the V2V links.

- Common reward

$$R_{(k,t)} = \lambda_1 \sum_{m \in \mathcal{M}} r_{m,(k,t)} + \lambda_2 \sum_{i \in \mathcal{L}} r_{i,(k,t)} |q_{i,(k,t)}^{\text{CAM}} > 0 + \sum_{i \in \mathcal{L}} Z |q_{i,(k,t)}^{\text{CAM}} = 0, \quad (9)$$

where Z is a tuned hyper-parameter encouraging early completion of transmission for CAM whose value is greater than the largest $r_{i,(k,t)}$ ever obtained [6].

- State transition probability

$$\Pr(s_{(k,t+1)} | s_{(k,t)}, a_{(k,t)}) = \Pr(G_{(k,t+1)} | G_{(k,t)}) \Pr(q_{(k,t+1)}^{\text{CAM}} | q_{(k,t)}^{\text{CAM}}, G_{(k,t)}, a_{(k,t)}), \quad (10)$$

where $\Pr(q_{(k,t+1)}^{\text{CAM}} | q_{(k,t)}^{\text{CAM}}, G_{(k,t)}, a_{(k,t)})$ can be derived from (7).

Note that, at the beginning of each control interval k , the queue length $q_{(k,0)}^{\text{CAM}}$ is reset to 1, and the actions taken during the past control intervals $k' < k$ do not affect the queue length at control interval k . Therefore, the time horizon of SIG is T communication intervals in a single control interval.

2) *MARL challenges*: All challenges present in the NFIG environment are exacerbated in the SIG environment. This is due to the presence of T communication intervals per episode, instead of just one, leading to the accumulation of relative overgeneralization and miscoordination errors over time steps.

In addition, a significant challenge for SIG lies in learning an optimal policy across a wide range of diverse states and being able to generalize this policy to unseen states. This difficulty arises from two main sources. First, fast fading introduces stochasticity into the environment, generating diverse channel conditions within the same episode. More importantly, vehicle mobility creates a broad spectrum of possible vehicular topologies, resulting in numerous potential path-loss values for V2V, V2I, and interference links. Even when fast fading is ignored, channel states remain fixed within an episode but vary across episodes due to changing topologies. While NFIG only needs to learn a policy tailored to a single fixed topology, SIG must develop a universal policy capable of making optimal decisions across all possible topologies, including those not encountered during training [33].

C. Partial Observable Stochastic Interference Game (POSIG)

1) *Environment model*: In SIG, it is assumed that each agent i can observe the global state $s_{(k,t)}$ in each communication interval (k, t) . This assumption is normally not realistic in practical scenarios. Instead, each agent i can only receive local observations consisting of partial information about the state $s_{(k,t)}$. This scenario can be formulated as a POSIG, which is defined by the same elements of SIG. Additionally, the observation for each agent $i \in \mathcal{L}$ is defined as [4]:

$$s_{i,(k,t)} = \{G_{i,(k,t)}, I_{i,(k,t-1)}, q_{i,(k,t)}^{\text{CAM}}, t\}, \quad (11)$$

where $G_{i,(k,t)} = \{G_{i,m,(k,t)}, G_{i,B,m,(k,t)}\}_{m \in \mathcal{M}}$ is the local observation of channel states at V2V transmitter i

in communication interval (k, t) . Moreover, $I_{i,(k,t-1)} = \{I_{i,m,(k,t-1)}\}_{m \in \mathcal{M}}$ is the received interference power at V2V receiver i over all subchannels at the previous communication interval $(k, t - 1)$.

2) *MARL challenges*: In addition to the MARL challenges in SIG, the *partial observability* in POSIG further increases the difficulty of solving the problems. Specifically, different global states can correspond to the same local observation, making it harder for agents to distinguish between them.

Having identified the key MARL challenges associated with each interference game, we next present the algorithms evaluated in this study to address these challenges.

V. ALGORITHMS

A. Independent Learning (IL)

In IL, each agent treats the other agents as part of the environment and uses the single agent RL algorithms to learn a policy.

1) Value-based:

IDQN In Independent DQN (IDQN), each agent has a pair of Q-network and target network and uses the off-policy DQN [34] for decentralized training in multi-agent environment.

Hysteric IDQN Hysteric IDQN is a variant of IDQN aimed at enhancing coordination in IL. Unlike standard IDQN, it employs two distinct learning rates based on the sign of the Temporal-Difference (TD) error [35].

2) Actor-critic:

IA2C In Independent synchronous Advantage Actor-Critic (IA2C), each agent has a pair of actor and critic networks, and uses the on-policy A2C [36] for decentralized training in multi-agent environment.

IPPO In IPPO, each agent uses the on-policy PPO [16] for decentralized training in multi-agent environment. Compared to IA2C, IPPO optimizes a surrogate objective by performing multiple update epochs within each training iteration.

B. Centralized Training and Decentralized Execution (CTDE)

In CTDE, it is assumed that global states and actions are available to the learning algorithms during the centralized training, while only local observations and actions are accessible to each agent during the decentralized execution.

1) *Value Decomposition*: In value-based RL, the joint Q-function is decomposed into individual utility functions during centralized training. Ideally, the IGM (Individual-Global-Max) condition should be satisfied, where the optimal global action that maximizes the joint Q-function corresponds to the set of optimal local actions that maximize each agent’s individual utility functions. During decentralized execution, each agent then uses its individual utility function to select actions. Value decomposition can fully resolve the multi-agent coordination problem if the IGM condition can be met. In partial observable environments, the individual utility functions are derived from local observations and it is normally much harder to satisfy the IGM condition.

VDN In Value Decomposition Networks (VDN) [37], the joint Q-function is the sum of individual utility functions.

QMIX In QMIX [38], the joint Q-function is a monotonic function of the individual utility functions. This monotonicity condition is more general than the additivity condition in VDN, allowing it to be satisfied by a broader range of tasks. However, both additivity and monotonicity are sufficient but not necessary conditions for satisfying the IGM principle. Consequently, QMIX’s performance may be limited in tasks that do not meet the monotonicity conditions.

2) *Centralized Critic Decentralized Actors*: In actor-critic RL, a centralized critic learns the joint value functions of global states or state-action pairs for all agents, while decentralized actors learn individual policies for each agent. In partial observable environments, these policies are conditioned on local observation-action history. Compared to IL, the centralized critic estimates the joint value functions rather than the expected joint value functions conditioned on each agent’s local observations or observation-action pairs. However, the multi-agent coordination problem still exists, as the policy gradient used for actor training is based on local rather than global actions. This issue is referred to as centralized-decentralized mismatch.

MAA2C Multi-agent A2C (MAA2C) [15] differs from IA2C by incorporating the global state into the critic, alongside local observations and previous actions, in environments with partial observability.

MAPPO The relationship between Multi-agent PPO (MAPPO) [39] and IPPO mirrors that between MAA2C and IA2C.

Table II summarizes the eight algorithms evaluated in this study. The MADDPG algorithm [27], another well-known CTDE actor-critic method, is excluded because it is primarily designed for continuous action spaces, whereas our C-V2X tasks involve discrete actions. Moreover, [15] shows that MADDPG underperforms relative to other algorithms across most evaluated games.

TABLE II: Summary of Evaluated MARL Algorithms

Algorithm	Type	Framework	On/Off-Policy
IDQN	Value-based	IL	Off-policy
Hys-IDQN	Value-based	IL	Off-policy
VDN	Value-based	CTDE	Off-policy
QMIX	Value-based	CTDE	Off-policy
IA2C	Actor-critic	IL	On-policy
IPPO	Actor-critic	IL	On-policy
MAA2C	Actor-critic	CTDE	On-policy
MAPPO	Actor-critic	CTDE	On-policy

VI. EXPERIMENT SETUP

We set up the simulated environment based on the evaluation methodology for the freeway case described in Annex A of 3GPP TR 36.885 [29], including the road configuration, V2V and V2I channel models, and the V2V traffic model. For

vehicle density and speed, we adopt three representative scenarios from ETSI TR 103 766 [30]: Scenario #1 (35 veh/km, 250 km/h), #3 (123 veh/km, 70 km/h), and #6 (500 veh/km, 50 km/h). The key parameters of the C-V2X environment are summarized in Table III, following existing works [6], [29]. For the reward functions, we set the weights with $\lambda_1:\lambda_2 = 1:9$ to prioritize CAM delivery [20]: $\lambda_1 = 0.1$, $\lambda_2 = 0.9$ for *NFIG*, and $\lambda_1 = 0.2$, $\lambda_2 = 1.8$, $Z = 0.5$ for *SIG/POSIG*.

TABLE III: Parameters of C-V2X Environment

Description	Value
Communication interval	1 ms
Control interval	100 ms
Carrier frequency	2 GHz
Total Bandwidth	4 MHz
V2I link/subchannel number	4
V2V link/agent number	{4, 8, 16}
Noise power	-114 dBm
V2I transmit power	23 dBm
V2V transmit power	{23, 10, 5, -100} dBm
BS antenna height	25 m
BS antenna gain	8 dBi
BS noise figure	5 dB
Vehicle antenna gain	3 dBi
Vehicle noise figure	9 dB
CAM size	$6 \times 1,060$ Bytes

A. Vehicle Positional Data Generation

We simulate a 2 km highway with three lanes in each direction (six lanes in total). Vehicle positional data is obtained from SUMO, an open-source traffic simulation platform that provides realistic vehicle movement data. We create datasets for all tasks with the goal of representing diverse interference conditions.

To capture realistic interference conditions while keeping computational complexity manageable, we adopt the following procedure. Initial topologies are generated by randomly placing the vehicles according to a spatial Poisson process at one end of the 2 km highway. All vehicles are confined within a distance of D m from the end of the highway, where D is given by the product of the vehicle density and the total number of vehicles.

Vehicles then travel at time-varying speeds with random lane changes, and positional data is sampled every 100 ms. This procedure is repeated under different vehicle densities and speeds. The training dataset consists of samples evenly distributed across the three density levels. Since training dataset size strongly affects policy generalization [33], we experimentally determined that 15,000 samples for 4-agent tasks and 60,000 for 8-/16-agent tasks yield the best performance.

The testing dataset comprises nine samples, generated by combining the three vehicle densities with three vehicle-to-BS distance levels—*close*, *mid*, and *far*—to represent typical interference conditions in highway scenarios. The number of subchannels is fixed at $M = 4$, while the number of agents varies across $L \in \{4, 8, 16\}$.

B. Learning Tasks

1) *NFIG*: *NFIG* is the simplest task, since the agents only need to learn the resource allocation policy for a given vehicle topology in a single time step. As discussed in Section IV.A.2), the main MARL challenges in *NFIG* are coordination difficulty and non-stationarity. These challenges often lead the learned policy to converge to a suboptimal Nash equilibrium rather than the optimal one. Since *NFIG* is essentially a matrix game, the coordination difficulty is heavily influenced by the structure of the matrix. We conduct nine experiments, each trained and tested on a single topology from the testing dataset. We fix $L=4$ agents, enabling exhaustive search to derive optimal policies. Since the *NFIG* task isolates coordination as the sole challenge, any performance gap relative to the optimum directly reflects agent coordination inefficiency.

2) *SIG*: *SIG* is a considerably more complex task compared with *NFIG*, involving a longer time horizon (multiple time steps rather than a single time step), fast fading, and diverse positional data. To investigate how these factors affect learning difficulty, we conduct ablation experiments on *SIG*.

a) *SIG Single Location with No Fast Fading (SL_NFF)*: We train and test in the *SIG* environment using a single positional data sample, similar to *NFIG*, and without fast fading. Comparing *NFIG* and *SIG SL_NFF* evaluates the impact of multiple time steps within an episode versus a single time step. In general, the impact of multiple time steps is influenced by two factors: the CAM size N_c and the time horizon T , which are set of 6×1060 bytes and 100, respectively, in this paper. Since the queue is typically exhausted within the first 20 time steps under a reasonable policy, we reduce the time horizon to 50 ms to accelerate training, while the learned policies remain valid for the full 100 ms horizon.

b) *SIG Single Location with Fast Fading (SL_FF)*: Based on *SIG SL_NFF*, we introduce fast fading to the wireless channels, adding stochasticity to state transitions. For the *SIG SL_FF* tasks, we further evaluate the ability of different algorithms to handle large action spaces by varying the number of agents, with $L \in \{4, 8, 16\}$.

c) *SIG Multiple Locations (ML)*: We use training dataset of 15,000 or 60,000 diverse positional samples along with a testing dataset of nine representative topologies, as described in Section VI.A. This setting corresponds to the standard *SIG* task outlined in Section IV.B, referred to as *SIG ML*. The comparison between *SIG SL_FF* and *SIG ML* highlights the difficulty of learning a policy that can handle a large number of varying topologies and generalize to unseen ones.

3) *POSIG*: In the *POSIG* environment, we use the same training and testing datasets as in the *SIG ML* tasks. Comparing *SIG ML* and *POSIG* isolates the effect of partial observability, where agents receive only local channel and queue states rather than the global information of all agents.

Table IV summarizes the properties and MARL challenges associated with each learning task.

C. Evaluation Protocol

Each algorithm was run on all five learning tasks (Table IV), using five random seeds for each task. We train all algorithms

TABLE IV: Overview of Properties and MARL Challenges of Learning Tasks. *FF* denotes Fast Fading, *Non-Stat.* denotes Non-Stationarity. *Robust./Gen.* denotes Robustness/Generalization.

Task	Properties			MARL Challenges				
	Steps	Agents	FF	Non-Stat.	Coordination	Large Action Space	Robust./Gen.	Partial Observability
<i>NFIG</i>	1	4		✓	✓			
<i>SIG SL_NFF</i>	50	4		✓	✓			
<i>SIG SL_FF</i>	50	4,8,16	✓	✓	✓	✓		
<i>SIG ML</i>	50	4,8,16	✓	✓	✓	✓	✓	
<i>POSIG</i>	50	4,8,16	✓	✓	✓	✓	✓	✓

for a number of environment time steps determined by task complexity and algorithm type, evaluating performance at regular intervals throughout training, resulting in a total of 100 evaluations per run. At each evaluation point, nine evaluation episodes were executed without exploration noise, and the average return across these episodes was calculated. For *SIG ML* and *POSIG* tasks, the nine evaluation episodes correspond to the nine test topologies; for other tasks, they are conducted on the single training topology.

To ensure a fair comparison between algorithms, we consider the inherent differences in sample efficiency between off-policy value-based algorithms (IDQN, Hys-IDQN, VDN, and QMIX) and on-policy actor-critic algorithms (IA2C, MAA2C, IPPO, and MAPPO) when determining the number of environment time steps used for training. Following [15], we empirically determine the number of time steps for each task such that further extensions yield no significant performance improvement.

Hyperparameters were tuned for each task category by evaluating each configuration over five seeds and selecting the best-performing one. Tables VII–X in Appendix A present the final values.

D. Performance Metrics

We normalize the returns for each task using the formula $\text{norm}_t G_t^a = (G_t^a - G_t^{\min}) / (G_t^{\max} - G_t^{\min})$, where G_t^{\min} is the return under a random policy in which each agent selects actions uniformly at random at each time step, and G_t^{\max} is obtained differently across tasks:

NFIG: Exhaustive search over the action space.

SIG SL: For 4-agent tasks, we perform per-step exhaustive search maximizing instantaneous V2V throughput, which approximates the optimal return while accounting for the early completion bonus Z in (9). For the 8- and 16-agent tasks, per-step exhaustive search is computationally infeasible. We therefore adopt a greedy iterative assignment algorithm that sequentially selects, for each agent, the subchannel–power pair maximizing V2V throughput, and repeats until no further improvement is possible.

SIG ML* and *POSIG: We reuse the “approximate optimal returns” obtained from *SIG SL_NFF* for each of the nine test topologies and average them.

For each algorithm, we report the maximum average test return achieved during training, computed over five independent runs with different random seeds. Table V presents these maximum returns along with their 95% confidence intervals. The top-performing algorithm in each task is indicated in bold.

VII. RESULTS AND DISCUSSIONS

A. *NFIG*

1) *Significance of coordination and non-stationarity challenges in single-step environment*: From Table V, of the 72 experiments (9 tasks \times 8 algorithms) for *NFIG*, 29 reached optimal performance across all five runs, with a maximum deviation of 7% (VDN and QMIX for 500_mid), showing most experiments achieve optimal or near-optimal results.

The main challenges in *NFIG* are coordination and non-stationarity. The coordination challenge arises from link interference: increasing an agent’s V2V transmit power improves its own throughput but reduces that of others sharing the same subchannel [40]. As a result, an agent’s best action is influenced by the actions of other agents at the same time step. While this could theoretically challenge advanced algorithms like QMIX, all methods—including simple IL approaches such as IDQN—achieve optimal performance in most of the *NFIG* tasks. We hypothesize this is because coordination penalties are low: the reward (sum throughput) remains non-negative for any joint action.

2) *Comparison between different vehicular topologies*:

Table V shows that some tasks/topologies are harder to learn optimal policies than others. For instance, 500_mid achieves the lowest average performance, with only MAPPO reaching the optimum, whereas simpler topologies like 35_mid and 123_close allow all algorithms to reach near-optimal performance (≥ 0.99).

To explain this variation, we define a *coordination difficulty score (CDS)*:

$$d = \frac{G_{NE}^{\max} - G_{NE}^{\min}}{G_{NE}^{\max}} + \frac{1 - G_{NE}^{\text{mean}}}{G_{NE}^{\max}}, \quad (12)$$

where G_{NE}^{\max} , G_{NE}^{\min} , and G_{NE}^{mean} are normalized equilibrium returns. As Table VI shows, CDS correlates negatively with performance (Pearson $r = -0.696$, $p = 0.037$): low-CDS topologies like 123_close (0.005) and 35_mid (0.002) achieve near-optimal results, while 500_mid (0.368) performs worst. This confirms that the topology-determined game structure primarily drives coordination difficulty.

The key insights from *NFIG* results are:

- **The challenges of coordination and non-stationarity are not pronounced in single-step environment.**
- **The coordination difficulty is primarily determined by the underlying game structure induced by topology-specific interference patterns: topologies with a single, high-value equilibrium are easy to learn, while those**

TABLE V: Maximum Normalized Returns and 95% Confidence Intervals over Five Seeds Across All Tasks

	Tasks/Algos.	IDQN	Hys-IDQN	VDN	QMIX	IA2C	MAA2C	IPPO	MAPPO
<i>NFIG</i>	35_far	0.97 ± 0.01	0.97 ± 0.00	0.97 ± 0.00	0.97 ± 0.00	0.94 ± 0.14	0.99 ± 0.02	0.97 ± 0.00	0.97 ± 0.02
	35_mid	1.00 ± 0.00							
	35_close	0.94 ± 0.04	0.97 ± 0.05	0.98 ± 0.04	1.00 ± 0.00	0.98 ± 0.04	1.00 ± 0.00	0.98 ± 0.04	1.00 ± 0.00
	123_far	0.97 ± 0.01	0.97 ± 0.00	0.97 ± 0.00	0.97 ± 0.00	0.97 ± 0.01	0.97 ± 0.03	0.97 ± 0.00	0.97 ± 0.01
	123_mid	0.99 ± 0.01	1.00 ± 0.01	1.00 ± 0.00	1.00 ± 0.00	0.98 ± 0.01	0.99 ± 0.01	0.99 ± 0.01	0.99 ± 0.01
	123_close	1.00 ± 0.00							
	500_far	0.99 ± 0.02	0.99 ± 0.02	1.00 ± 0.00	1.00 ± 0.00	1.00 ± 0.00	0.99 ± 0.02	0.99 ± 0.02	0.97 ± 0.07
	500_mid	0.97 ± 0.05	0.95 ± 0.04	0.93 ± 0.00	0.93 ± 0.00	0.95 ± 0.06	0.97 ± 0.05	1.00 ± 0.00	1.00 ± 0.00
	500_close	0.99 ± 0.01	0.98 ± 0.01	1.00 ± 0.00	1.00 ± 0.00	0.99 ± 0.01	0.98 ± 0.01	0.98 ± 0.01	0.99 ± 0.01
	Average	0.98 ± 0.02	0.98 ± 0.01	0.98 ± 0.02	0.99 ± 0.02	0.98 ± 0.02	0.99 ± 0.01	0.99 ± 0.01	0.99 ± 0.01
<i>Without Fast Fading (NFF) 4ag</i>									
<i>SIG SL</i>	35_far	0.99 ± 0.02	0.99 ± 0.01	1.00 ± 0.01	0.99 ± 0.01	0.99 ± 0.00	0.99 ± 0.00	0.94 ± 0.04	0.94 ± 0.04
	35_mid	0.88 ± 0.04	0.91 ± 0.07	1.00 ± 0.00	1.00 ± 0.00	1.00 ± 0.00	0.99 ± 0.02	0.96 ± 0.04	0.99 ± 0.04
	35_close	0.82 ± 0.08	0.87 ± 0.08	0.97 ± 0.01	0.97 ± 0.01	0.94 ± 0.00	0.99 ± 0.00	0.96 ± 0.03	0.98 ± 0.04
	123_far	0.98 ± 0.01	0.98 ± 0.01	0.99 ± 0.01	0.99 ± 0.00	0.98 ± 0.03	0.97 ± 0.03	0.96 ± 0.01	0.97 ± 0.02
	123_mid	0.99 ± 0.00	0.99 ± 0.00	0.99 ± 0.01	0.99 ± 0.00	0.97 ± 0.02	0.97 ± 0.02	0.98 ± 0.01	0.98 ± 0.02
	123_close	0.98 ± 0.01	1.00 ± 0.01	1.00 ± 0.01	1.00 ± 0.00	0.99 ± 0.01	1.00 ± 0.01	1.00 ± 0.01	0.99 ± 0.02
	500_far	1.00 ± 0.00	1.00 ± 0.01	1.00 ± 0.01	1.00 ± 0.00	0.99 ± 0.03	1.00 ± 0.01	0.97 ± 0.03	0.99 ± 0.01
	500_mid	0.95 ± 0.05	0.93 ± 0.04	0.99 ± 0.01	1.00 ± 0.01	0.97 ± 0.03	0.98 ± 0.03	0.98 ± 0.02	0.98 ± 0.04
	500_close	0.97 ± 0.02	0.97 ± 0.03	1.00 ± 0.01	1.00 ± 0.01	0.98 ± 0.03	0.99 ± 0.03	0.98 ± 0.02	0.96 ± 0.01
	Average	0.95 ± 0.06	0.96 ± 0.05	0.99 ± 0.01	0.99 ± 0.01	0.98 ± 0.01	0.99 ± 0.01	0.97 ± 0.02	0.98 ± 0.02
<i>With Fast Fading (FF) 4ag</i>									
Average	0.95 ± 0.04	0.98 ± 0.01	0.99 ± 0.03	0.99 ± 0.03	0.99 ± 0.03	1.00 ± 0.03	0.99 ± 0.02	0.99 ± 0.02	
<i>With Fast Fading (FF) 8ag</i>									
Average	0.95 ± 0.04	0.95 ± 0.05	0.99 ± 0.03	0.98 ± 0.04	0.98 ± 0.05	0.98 ± 0.06	1.00 ± 0.02	1.00 ± 0.02	
<i>With Fast Fading (FF) 16ag</i>									
Average	0.84 ± 0.03	0.84 ± 0.04	0.96 ± 0.06	0.95 ± 0.06	0.90 ± 0.03	0.90 ± 0.04	0.99 ± 0.03	1.00 ± 0.02	
<i>SIG ML</i>	4ag	0.59 ± 0.07	0.57 ± 0.09	0.61 ± 0.11	0.59 ± 0.11	0.76 ± 0.03	0.76 ± 0.04	0.80 ± 0.04	0.80 ± 0.04
	8ag	0.29 ± 0.06	0.27 ± 0.05	0.43 ± 0.11	0.43 ± 0.03	0.58 ± 0.03	0.58 ± 0.03	0.61 ± 0.02	0.61 ± 0.02
	16ag	-0.22 ± 0.11	-0.21 ± 0.05	-0.09 ± 0.21	0.00 ± 0.20	0.35 ± 0.05	0.34 ± 0.07	0.54 ± 0.02	0.54 ± 0.01
<i>POSIG</i>	4ag	0.71 ± 0.02	0.69 ± 0.03	0.78 ± 0.01	0.77 ± 0.03	0.79 ± 0.05	0.88 ± 0.04	0.88 ± 0.02	0.88 ± 0.01
	8ag	0.66 ± 0.04	0.67 ± 0.02	0.62 ± 0.06	0.62 ± 0.03	0.60 ± 0.03	0.73 ± 0.02	0.79 ± 0.02	0.82 ± 0.02
	16ag	0.52 ± 0.08	0.49 ± 0.07	0.47 ± 0.01	0.48 ± 0.06	0.51 ± 0.03	0.61 ± 0.02	0.69 ± 0.04	0.74 ± 0.05

 TABLE VI: Coordination Difficulty Score (CDS) and average performance across all algorithms for each topology. The CDS is computed from the statistics of Nash equilibria for *NFIG*, with lower values indicating easier coordination. Avg. Perf. denotes the mean normalized return across all eight algorithms for each topology, as reported in Table V.

Topology	CDS	Avg. Perf.	
		<i>NFIG</i>	<i>SIG SL_NFF</i>
35_far	0.316	0.97	0.99
35_mid	0.002	1.00	0.98
35_close	0.121	0.98	0.94
123_far	0.070	0.97	0.97
123_mid	0.028	0.99	0.98
123_close	0.005	1.00	0.99
500_far	0.335	0.99	0.99
500_mid	0.368	0.96	0.97
500_close	0.034	0.99	0.98

with multiple heterogeneous equilibria introduce coordination ambiguity and hinder learning.

B. SIG-SL

1) *Significance of coordination and non-stationarity challenges in multi-step environment:* We compare *NFIG* and *SIG SL_NFF* to assess whether the coordination and non-stationarity challenges present in single-step settings become more severe in multi-step environments. Table V shows that among 72 experiments for *SIG SL_NFF*, 17 reached “approximate optimal” performance across all five runs, fewer than in *NFIG*. The maximum deviation is 18% (IDQN on 35_close), higher than in *NFIG*, yet 64 of 72 experiments deviate by less than 5%, indicating most results remain near-optimal.

Extending the time horizon from one to 50 steps could potentially exacerbate coordination difficulty and non-stationarity through the accumulation of errors over multiple time steps. However, comparing performance across topologies (Table VI), eight of nine show performance differences within ±2% between *NFIG* and *SIG SL_NFF*, suggesting multi-step decision making does not significantly impact overall performance. We attribute this to the fact that the coordination structure—determined by the underlying interference patterns—remains consistent across time steps within an episode.

2) *Comparison between different algorithms:* QMIX (0.99) and VDN (0.99) consistently outperform Hys-IDQN (0.96)

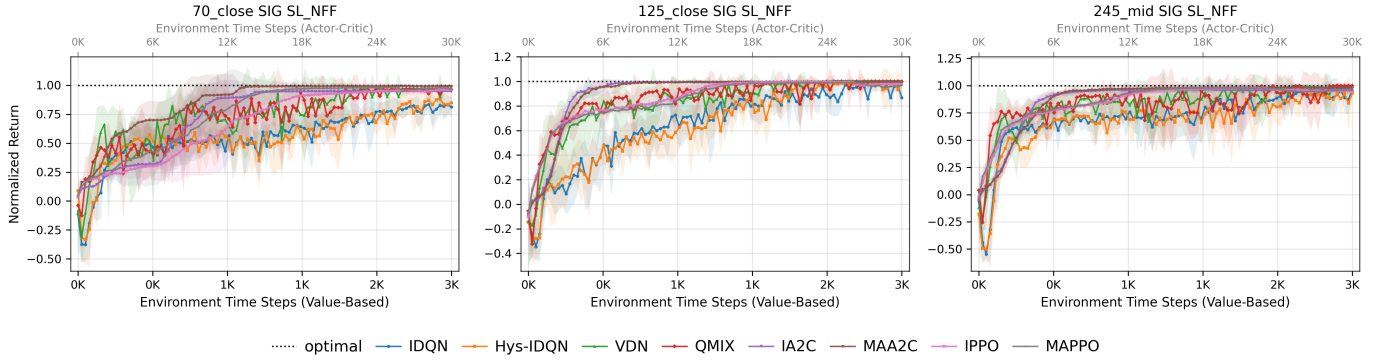


Fig. 1: Normalized returns in selected *SIG SL_NFF* tasks. Shaded areas represent the 95% CI over five seeds.

and IDQN (0.95), highlighting the advantage of value-decomposition methods in capturing the relationship between individual and joint action values. In contrast, actor-critic CTDE algorithms show little advantage over their IL counterparts: MAPPO (0.98) and MAA2C (0.99) perform similarly to IPPO (0.97) and IA2C (0.98). This is expected, as the global state is available to all agents in *SIG SL* tasks, making CTDE and IL actor-critic algorithms nearly equivalent under parameter sharing.

3) *Impact of fast fading*: We compare *SIG SL_NFF* and *SIG SL_FF* to assess the impact of fast fading on algorithm performance. Table V shows that average performance remains similar across all algorithms with and without fast fading (*SIG SL_NFF*: 0.95–0.99, *SIG SL_FF*: 0.95–1.00), with some—like Hys-IDQN, IA2C, IPPO, and MAPPO—even performing slightly better under fast fading. This indicates that moderate stochasticity in the wireless channels does not degrade performance.

4) *Impact of large action space*: We compare *SIG SL_FF* in 4-, 8-, and 16-agent settings to assess how increasing the action space affects learning. Table V shows that performance is stable from four to eight agents, with most algorithms achieving near-optimal returns. At 16 agents, differences emerge: value-based IL algorithms (IDQN, Hys-IDQN: 0.84) drop most, PPO-based methods (IPPO, MAPPO: 1.00) remain near-optimal, and value decomposition (VDN: 0.96, QMIX: 0.95) and A2C variants (IA2C, MAA2C: 0.90) fall in between.

This trend reflects how different algorithms cope with non-stationarity induced by joint-action space growth. As the number of agents increases, each agent’s environment depends on an increasingly large and evolving joint policy. Consequently, replay-buffer samples collected under previous joint policies become increasingly inconsistent, leading to performance degradation in value-based methods. Value decomposition approaches partially mitigate this effect through structured factorization but remain sensitive to stale replay buffers. In contrast, actor-critic methods rely on on-policy updates and thus naturally adapt to the evolving joint policy. PPO further stabilizes learning by constraining policy updates via its clipped objective, explaining its superior scalability.

The key insights from *SIG SL* results are:

- **Multi-step decision-making, fast fading, and larger action space have limited impact on performance.**

- **In fully observable environments, value-based CTDE methods (VDN, QMIX) excel at coordination through value decomposition at small scales, whereas CTDE offers no clear advantage for actor-critic methods. As the number of agents increases, however, the performance of value-based methods degrades, while PPO-based actor-critic algorithms maintain near-optimal performance, demonstrating superior scalability.**

C. *SIG-ML*

1) *Significance of robustness and generalization challenges*: Compared with *SIG SL_FF*, which trains on a single topology, *SIG ML* trains on a much larger, more diverse dataset (15,000 samples for 4 agents; 60,000 for 8/16 agents) while evaluating on the same nine representative topologies (Section VI.A). We tested three dataset-sampling methods—random, consecutive, and random batches of ten consecutive topologies—and selected random sampling as best.

Table V shows substantial performance degradation in *SIG ML*: in the 4-agent case, drops range from 19.19% (IPPO/MAPPO) to 41.84% (Hys-IDQN), with larger drops for 8- and 16-agent settings.

Two main challenges drive this: (1) robustness—learning policies that perform well across diverse topologies; and (2) generalization—to unseen topologies. To isolate these effects, we conduct ablations with IDQN and IPPO in the 16-agent setting. We test performance on nine samples randomly drawn from the training dataset (included in training) and compare it with the original nine representative topologies (excluded from training). On these training samples, IDQN scores 0.36 ± 0.03 and IPPO 0.56 ± 0.05 , well below their *SIG SL_FF* performance (0.84, 0.99), showing that robustness—learning a policy that performs well across diverse topologies—is a major factor in performance degradation. The additional drop to the excluded topologies is minor for IPPO ($0.56 \rightarrow 0.54$), suggesting generalization is easier once robustness is addressed. In contrast, IDQN drops further ($0.36 \rightarrow -0.22$), indicating generalization remains a critical challenge for this algorithm.

Finally, since our results on *SIG SL_FF* show that performance does not degrade substantially with increasing action space, the primary cause of performance deterioration at larger scales is not action-space expansion but the growing difficulty

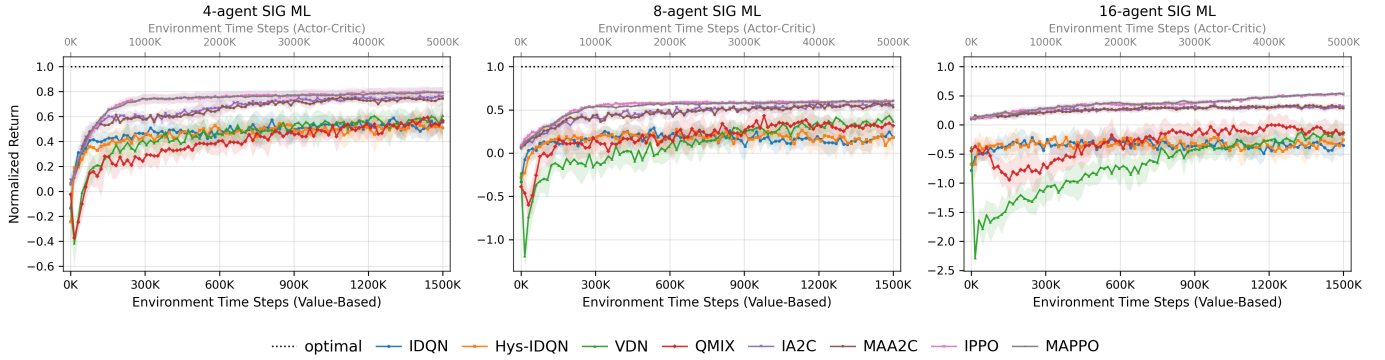


Fig. 2: Normalized returns in selected *SIG ML* tasks. Shaded areas represent the 95% CI over five seeds.

of robustness and generalization. As the number of agents increases, the diversity of interference patterns grows rapidly, making it increasingly challenging for learned policies to generalize to unseen topologies.

2) Comparison between different algorithms:

a) *Value-based vs. Actor-Critic*: As shown in Table V, actor-critic algorithms clearly outperform value-based algorithms in *SIG ML*. For example, in the 4-agent setting, IPPO and MAPPO achieve the highest performance (0.80), followed by IA2C and MAA2C (0.76), whereas value-based algorithms perform significantly lower (VDN: 0.61, QMIX: 0.59, IDQN: 0.59, Hys-IDQN: 0.57). As the number of agents increases, this gap widens further, with value-based algorithms collapsing to near-zero or negative returns at 16 agents while actor-critic algorithms maintain positive performance.

b) *IL vs. CTDE*: For value-based algorithms, CTDE algorithms (VDN and QMIX) outperform their IL counterparts (IDQN and Hys-IDQN), with the advantage increasing as the number of agents grows (4ag: 0.02–0.04, 8ag: 0.14–0.16, 16ag: 0.13–0.21). This suggests that value decomposition partially mitigates generalization challenges, although it remains insufficient to close the gap with actor-critic methods. For actor-critic algorithms, CTDE methods (MAPPO, MAA2C) perform similarly to their IL counterparts (IPPO, IA2C) across all scales, consistent with the observations in *SIG SL*.

The key insights from *SIG ML* results are:

- Learning a policy that can adapt across diverse vehicular topologies and generalize to unseen ones are critical challenges in C-V2X RRA problems.
- Actor-critic algorithms exhibit significantly stronger robustness and generalization capabilities than value-based algorithms.

D. POSIG

1) *Significance of partial observability challenge*: As shown in Table V, *POSIG* outperforms *SIG ML* across all algorithms and tasks, with gains particularly pronounced for value-based methods. In the 8-agent setting, value-based algorithms improve by 44%–148%, and in the 16-agent setting, they recover from near-zero or negative returns to above 0.47. Actor-critic methods, by contrast, show only modest improvements.

Although agents in *POSIG* operate under partial observability, this does not appear to be a limiting factor. We attribute the performance gains to the reduced state dimension: the global state in *SIG ML* scales quadratically with the number of agents due to pairwise interference terms, whereas the local observations in *POSIG* remain fixed. We hypothesize that much of the high-dimensional global state is redundant and that compact local observations better capture topology-relevant information. However, since *POSIG* still underperforms *SIG SL_FF*, robustness and generalization challenges remain.

To further assess the impact of partial observability, we compared fully connected (FC) and recurrent (Gated Recurrent Unit (GRU)) architectures and found little benefit from recurrence, further indicating that partial observability is not a major bottleneck in *POSIG*. Accordingly, we use FC networks for all tasks and algorithms in our experiments.

2) Comparison between Different Algorithms:

a) *Value-based vs. Actor-Critic*: As shown in Table V, actor-critic algorithms consistently outperform value-based algorithms in *POSIG*, in alignment with the findings for *SIG ML*. IPPO and MAPPO achieve the highest performance across all agent scales (4-agent: 0.88; 8-agent: 0.79–0.82; 16-agent: 0.69–0.74), followed by MAA2C and IA2C. In contrast, value-based algorithms exhibit lower performance, with the gap widening as the number of agents increases.

b) *IL vs. CTDE*: For value-based algorithms, CTDE algorithms (VDN: 0.78, QMIX: 0.77) outperform their IL counterparts (IDQN: 0.71, Hys-IDQN: 0.69) in the 4-agent setting. However, this advantage diminishes at larger scales, with VDN and QMIX performing comparably to or slightly worse than IDQN and Hys-IDQN in the 8-agent and 16-agent settings. This reversal occurs because individual Q-functions learned from local observations violate the IGM assumption more severely, and the resulting errors compound through the mixing network as the number of agents increases.

For actor-critic algorithms, CTDE provides a consistent advantage under partial observability: MAA2C outperforms IA2C across all scales (4-agent: 0.88 vs. 0.79; 8-agent: 0.73 vs. 0.60; 16-agent: 0.61 vs. 0.51), and MAPPO maintains a modest advantage over IPPO as the number of agents increases.

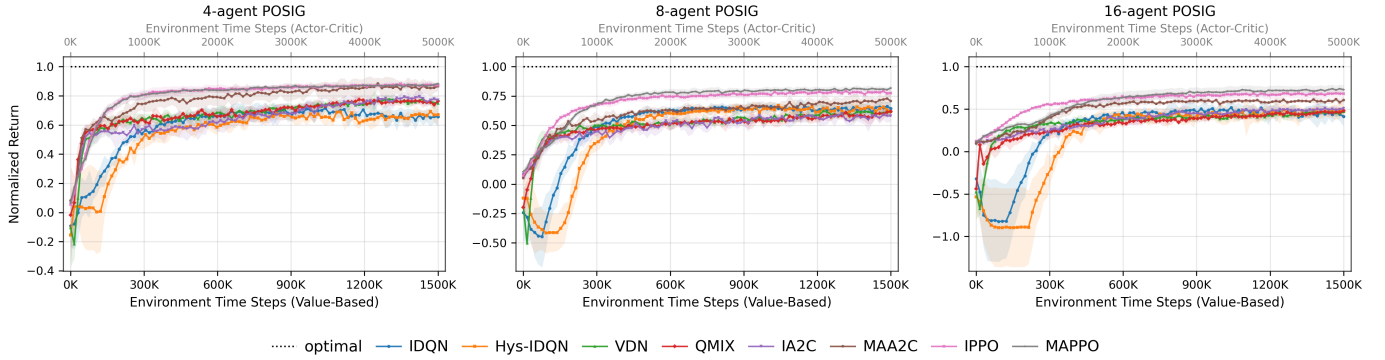


Fig. 3: Normalized returns in selected *POSIG* tasks. Shaded areas represent the 95% CI over five seeds.

The convergence curves of all algorithms for *SIG SL_{NFF}*, *SIG ML*, and *POSIG* tasks are shown in Fig. 1, Fig. 2, and Fig. 3, respectively. It can be observed that actor-critic algorithms consistently display stable, monotonic improvements, whereas value-based methods exhibit pronounced oscillations and higher variance. This instability arises because value-based learning repeatedly bootstraps from non-stationary Q-targets, making updates sensitive to short-term reward fluctuations.

The key insights from *POSIG* results are:

- **Partial observability is not a critical limitation; instead, high-dimensional global states hinder learning in diverse-topology settings.**
- **In partially observable environments, CTDE benefits actor-critic algorithms but provides diminishing or negative advantage for value-based algorithms at larger scales.**
- **MAPPO achieves the best or jointly best performance across all tasks, while IPPO offers comparable performance with better scalability.**

VIII. CONCLUSION AND FUTURE WORKS

In this paper, we conceived a series of interference games for RRA in C-V2X networks to isolate main MARL challenges and benchmarked the performance of eight classical MARL algorithms. Through our experiments, we identified the following key insights.

- The most critical MARL challenge in the C-V2X environment is not the well-known issues of non-stationary environment, coordination challenges, large action space, or partial observability, but rather learning policies that can adapt to a wide range of vehicular topologies and generalize to unseen ones.
- Both value-based and actor-critic algorithms perform well in simplified tasks where an agent learns an optimal policy for a single, fixed vehicular topology. However, in more complex, realistic tasks involving diverse vehicular topologies, actor-critic algorithms achieve higher performance and exhibit smoother learning curves.
- For actor-critic algorithms, PPO consistently outperforms A2C. Incorporating a centralized critic does not yield significant gains for MAPPO compared to IPPO; given the limited scalability of centralized critics, IPPO represents the more practical choice.

These insights offer guidance for future work. Although value-based IL is the most common MARL approach for C-V2X RRA, greater attention should be given to actor-critic algorithms due to their superior performance. IPPO is recommended as a baseline for its balance of performance and scalability.

A critical challenge is enabling policies to generalize across diverse vehicular topologies. Experimental results comparing *SIG SL* with *SIG ML* and *POSIG* show that standard RL algorithms perform well when trained on a single topology, but their performance degrades significantly—even on seen tasks—when exposed to many different topologies. The vehicular topology—and consequently the path loss of all links—affects the queue transition dynamics. While topologies remain fixed within an episode, they vary across episodes, making the *SIG ML* and *POSIG* environments a continuum of related tasks, each with distinct dynamics. Given the impracticality of learning a separate policy for every possible transition function, it is highly desirable for the learned policy to enable *zero-shot transfer*, solving both seen and unseen tasks at runtime without additional training. These insights are also applicable to advanced physical-layer techniques, including millimeter-wave (mmWave) and massive multiple-input multiple-output (MIMO) systems.

We hypothesize that a primary reason for the limited robustness and generalization is that channel gains and interference power, as currently represented in the state, are not efficient for differentiating between topologies. The performance advantage of *POSIG* over *SIG ML* further suggests that including all channel gains in the state can be detrimental to learning. Although some efforts have been made to learn more efficient state representations using GNNs [11] and to improve generalization through meta-learning [12], further research is needed. The *SIG SL* baselines presented in this paper offer a methodology for evaluating how effectively an algorithm can tackle this issue.

APPENDIX A HYPERPARAMETERS

The hyperparameters used in all experiments are given in Tables VII–X.

TABLE VII: *NFIG / SIG SL* Hyperparameters for Value-Based Algorithms

Hyperparameter	IDQN	Hys-IDQN	VDN	QMIX
actor/critic hidden dimension (FC)	128	128	128	128
learning rate	3×10^{-5}	3×10^{-5}	3×10^{-5}	3×10^{-5}
mixing network learning rate	-	-	-	1×10^{-6}
hysteretic learning rate	-	$\alpha=1.0, \beta=0.2$	-	-
discount factor (γ)	0.9	0.9	0.9	0.9
batch size	64	64	64	64
target update (soft)	5×10^{-3}	5×10^{-3}	5×10^{-3}	5×10^{-3}
training episodes	50,000 / 3,000	50,000 / 3,000	50,000 / 3,000	50,000 / 3,000
epsilon anneal steps (linear)	40,000 / 2,400	40,000 / 2,400	40,000 / 2,400	40,000 / 2,400
parameter sharing	False	False	False	False

Note: Values shown as a/b indicate different settings for *NFIG / SIG SL* respectively. Single values apply to both.

TABLE VIII: *NFIG / SIG SL* Hyperparameters for Actor-Critic Algorithms

Hyperparameter	IA2C	MAA2C	IPPO	MAPPO
hidden dimension (FC)	128	128	128	128
actor learning rate (α)	2×10^{-4}	2×10^{-4}	4×10^{-4}	4×10^{-4}
critic learning rate (β)	2×10^{-4}	2×10^{-4}	6×10^{-4}	6×10^{-4}
discount factor (γ)	0.9	0.9	0.99	0.99
batch size	8	8	256	256
mini-batches	-	-	4	4
target update (soft)	0.01	0.01	-	-
PPO epochs	-	-	10	10
entropy coefficient	-	-	0.001	0.001
training episodes	50,000 / 30,000	50,000 / 30,000	50,000 / 30,000	50,000 / 30,000
parameter sharing	False	False	True	True

Note: Values shown as a/b indicate different settings for *NFIG / SIG SL* respectively. Single values apply to both.

TABLE IX: *SIG ML / POSIG* Hyperparameters for Value-Based Algorithms

Hyperparameter	IDQN	Hys-IDQN	VDN	QMIX
hidden dimension (FC)	128	128	128	128
learning rate	$10^{-5} / 10^{-6}$	$10^{-5} / 10^{-6}$	10^{-5}	10^{-5}
mixing network learning rate	-	-	-	10^{-6}
hysteretic learning rate	-	$\alpha=1.0, \beta=0.2$	-	-
discount factor (γ)	0.9	0.9	0.9	0.9
batch size	64	64	64	64
target update (soft)	5×10^{-3}	5×10^{-3}	5×10^{-3}	5×10^{-3}
training episodes	30,000	30,000	30,000	30,000
epsilon anneal steps (linear)	24,000	24,000	24,000	24,000
parameter sharing	False	False	False	False

Note: Values shown as a/b indicate different settings for *SIG ML / POSIG* respectively. Single values apply to both.

TABLE X: *SIG ML / POSIG* Hyperparameters for Actor-Critic Algorithms

Hyperparameter	IA2C	MAA2C	IPPO	MAPPO
actor/critic hidden dimension (FC)	128	128	128	128
actor learning rate (α)	5×10^{-4}	5×10^{-4}	4×10^{-4}	4×10^{-4}
critic learning rate (β)	5×10^{-4}	5×10^{-4}	6×10^{-4}	6×10^{-4}
discount factor (γ)	0.9	0.9	0.99	0.99
batch size	8	8	256	256
mini-batches	-	-	4	4
target update (soft)	0.01	0.01	-	-
PPO epochs	-	-	10	10
entropy coefficient	-	-	0.001	0.001
training episodes	100,000	100,000	100,000	100,000
parameter sharing	True	True	True	True

Note: Values shown as a/b indicate different settings for *SIG ML / POSIG* respectively. Single values apply to both.

REFERENCES

- [1] S. Wang, P. Maheshwari, L. Lei, J. Mei, and K. Zheng, "Multi-agent drl for resource allocation in vehicular networks: A comparative study," in *ICC 2025 - IEEE International Conference on Communications, 2025*, pp. 1936–1941.
- [2] Y. Liu, J. Wu, and J. Zhang, "Recent advances and future trends in vehicular communication systems: A comprehensive survey," *IEEE Communications Surveys & Tutorials*, vol. 23, no. 1, pp. 38–84, 2021.
- [3] L. Lei, H. Xu, X. Xiong, K. Zheng, W. Xiang, and X. Wang, "Multiuser resource control with deep reinforcement learning in iot edge computing," *IEEE Internet of Things Journal*, vol. 6, no. 6, pp. 10119–10133, 2019.
- [4] H. Ye and G. Y. Li, "Deep reinforcement learning based resource allocation for v2v communications," *IEEE Transactions on Vehicular Technology*, vol. 68, no. 4, pp. 3163–3173, 2019.
- [5] S. V. Albrecht, F. Christianos, and L. Schäfer, *Multi-Agent Reinforcement Learning: Foundations and Modern Approaches*. MIT Press, 2024. [Online]. Available: <https://www.marl-book.com>
- [6] L. Liang, H. Ye, and G. Y. Li, "Spectrum sharing in vehicular networks based on multi-agent reinforcement learning," *IEEE Journal on Selected Areas in Communications*, vol. 37, no. 10, pp. 2282–2292, 2019.
- [7] P. Xiang, H. Shan, M. Wang, Z. Xiang, and Z. Zhu, "Multi-agent RL enables decentralized spectrum access in vehicular networks," *IEEE Transactions on Vehicular Technology*, vol. 70, no. 10, pp. 10750–10762, 2021.
- [8] P. Xiang, H. Shan, Z. Su, Z. Zhang, C. Chen, and E.-P. Li, "Multi-agent reinforcement learning-based decentralized spectrum access in vehicular networks with emergent communication," *IEEE Communications Letters*, vol. 27, no. 1, pp. 195–199, 2023.
- [9] Y. Ding, Y. Huang, L. Tang, X. Qin, and Z. Jia, "Resource allocation in V2X communications based on multi-agent reinforcement learning with attention mechanism," *Mathematics*, vol. 10, no. 19, p. Art. no. 3415, 2022. [Online]. Available: <https://www.mdpi.com/2227-7390/10/19/3415>
- [10] H. Zhang, C. Lu, H. Tang, X. Wei, L. Liang, L. Cheng, W. Ding, and Z. Han, "Mean-field aided multi-agent reinforcement learning for resource allocation in vehicular networks," *IEEE Internet of Things Journal*, 2022.
- [11] M. Ji, Q. Wu, P. Fan, N. Cheng, W. Chen, J. Wang, and K. B. Letaief, "Graph neural networks and deep reinforcement learning based resource allocation for v2x communications," 2025. [Online]. Available: <https://arxiv.org/abs/2407.06518>
- [12] Y. Yuan, G. Zheng, K.-K. Wong, and K. B. Letaief, "Meta-reinforcement learning based resource allocation for dynamic v2x communications," *IEEE Transactions on Vehicular Technology*, vol. 70, no. 9, pp. 8964–8977, 2021.
- [13] L. Lei, T. Liu, K. Zheng, and X. Shen, "Multitimescale control and communications with deep reinforcement learning—part ii: Control-aware radio resource allocation," *IEEE Internet of Things Journal*, vol. 11, no. 9, pp. 15475–15489, 2023.
- [14] A. Oroojlooy and D. Hajinezhad, "A review of cooperative multi-agent deep reinforcement learning," *Applied Intelligence*, vol. 53, no. 11, pp. 13677–13722, 2023.
- [15] G. Papoudakis, F. Christianos, L. Schäfer, and S. V. Albrecht, "Benchmarking multi-agent deep reinforcement learning algorithms in cooperative tasks," *arXiv preprint arXiv:2006.07869*, 2020.
- [16] J. Schulman, F. Wolski, P. Dhariwal, A. Radford, and O. Klimov, "Proximal policy optimization algorithms," *arXiv preprint arXiv:1707.06347*, 2017. [Online]. Available: <https://arxiv.org/abs/1707.06347>.
- [17] J. Tian, Y. Shi, X. Tong, S. Chen, and R. Zhao, "Deep reinforcement learning based resource allocation with heterogeneous qos for cellular v2x," in *2023 IEEE Wireless Communications and Networking Conference (WCNC)*, 2023, pp. 1–6.
- [18] J. Gui, L. Lin, X. Deng, and L. Cai, "Spectrum-energy-efficient mode selection and resource allocation for heterogeneous v2x networks: A federated multi-agent deep reinforcement learning approach," *IEEE/ACM Transactions on Networking*, vol. 32, no. 3, pp. 2689–2704, 2024.
- [19] M. Jamal, Z. Ullah, M. Naeem, M. Abbas, and A. Coronato, "A hybrid multi-agent reinforcement learning approach for spectrum sharing in vehicular networks," *Future Internet*, vol. 16, no. 5, p. 152, 2024.
- [20] K. Xu, S. Zhou, and G. Y. Li, "Federated reinforcement learning for resource allocation in v2x networks," *IEEE Journal of Selected Topics in Signal Processing*, 2024.
- [21] Z. Shao, Q. Wu, P. Fan, N. Cheng, Q. Fan, and J. Wang, "Semantic-aware resource allocation based on deep reinforcement learning for 5g-v2x hetnets," *IEEE Communications Letters*, 2024.
- [22] Y. Xu, K. Zhu, H. Xu, and J. Ji, "Deep reinforcement learning for multi-objective resource allocation in multi-platoon cooperative vehicular networks," *IEEE Transactions on Wireless Communications*, 2023.
- [23] Y. Song, Y. Xiao, and J. Liu, "Enabling adaptive optimization of energy efficiency and quality of service in nr-v2x communications via multiagent deep reinforcement learning," *IEEE Internet of Things Journal*, vol. 12, no. 4, pp. 4022–4037, 2025.
- [24] M. Parvini, M. R. Javan, N. Mokari, B. Abbasi, and E. A. Jorswieck, "Aoi-aware resource allocation for platoon-based c-v2x networks via multi-agent multi-task reinforcement learning," *IEEE Transactions on Vehicular Technology*, vol. 72, no. 8, pp. 9880–9896, 2023.
- [25] W. Zhang, Q. Wu, P. Fan, K. Wang, N. Cheng, W. Chen, and K. B. Letaief, "Semantic-aware resource management for c-v2x platooning via multi-agent reinforcement learning," 2025. [Online]. Available: <https://arxiv.org/abs/2411.04672>
- [26] L. Lei, Y. Tan, K. Zheng, S. Liu, K. Zhang, and X. Shen, "Deep reinforcement learning for autonomous internet of things: Model, applications and challenges," *IEEE Communications Surveys & Tutorials*, vol. 22, no. 3, pp. 1722–1760, 2020.
- [27] R. Lowe, Y. I. Wu, A. Tamar, J. Harb, O. Pieter Abbeel, and I. Mordatch, "Multi-agent actor-critic for mixed cooperative-competitive environments," *Advances in neural information processing systems*, vol. 30, 2017.
- [28] T. P. Lillicrap, J. J. Hunt, A. Pritzel, N. Heess, T. Erez, Y. Tassa, D. Silver, and D. Wierstra, "Continuous control with deep reinforcement learning," in *International Conference on Learning Representations*, 2016.
- [29] "Technical Specification Group Radio Access Network; Study LTE-Based V2X Services; (Release 14)," 3rd Generation Partnership Project (3GPP), Tech. Rep. 3GPP TR 36.885 V14.0.0, Jun. 2016, release 14. [Online]. Available: https://www.3gpp.org/ftp/Specs/archive/36_series/36.885/36885-f00.zip
- [30] "Intelligent transport systems (its); pre-standardization study on co-channel co-existence between ieee- and 3gpp- based its technologies in the 5 855 mhz - 5 925 mhz frequency band," *European Telecommunications Standards Institute (ETSI) Technical Report*, vol. TR 103 766, no. V1.1.1, 2021.
- [31] L. Lei, Y. Kuang, N. Cheng, X. Shen, Z. Zhong, and C. Lin, "Delay-optimal dynamic mode selection and resource allocation in device-to-device communications—part ii: Practical algorithm," *IEEE Transactions on Vehicular Technology*, vol. 65, no. 5, pp. 3491–3505, 2015.
- [32] E. Wei and S. Luke, "Lenient learning in independent-learner stochastic cooperative games," *Journal of Machine Learning Research*, vol. 17, no. 84, pp. 1–42, 2016. [Online]. Available: <http://jmlr.org/papers/v17/15-417.html>
- [33] K. Cobbe, C. Hesse, J. Hilton, and J. Schulman, "Leveraging procedural generation to benchmark reinforcement learning," in *Proceedings of the 37th International Conference on Machine Learning*, ser. Proceedings of Machine Learning Research, vol. 119. PMLR, 2020, pp. 2048–2056.
- [34] V. M. et al., "Human-level control through deep reinforcement learning," *Nature*, vol. 518, pp. 529–533, 2015.
- [35] L. Matignon, G. J. Laurent, and N. Le Fort-Piat, "Hysteretic q-learning: an algorithm for decentralized reinforcement learning in cooperative multi-agent teams," in *2007 IEEE/RSJ International Conference on Intelligent Robots and Systems*. IEEE, 2007, pp. 64–69.
- [36] V. Mnih, A. P. Badia, M. Mirza, A. Graves, T. Lillicrap, T. Harley, D. Silver, and K. Kavukcuoglu, "Asynchronous methods for deep reinforcement learning," in *Proceedings of The 33rd International Conference on Machine Learning*, ser. Proceedings of Machine Learning Research, vol. 48. PMLR, 2016, pp. 1928–1937.
- [37] P. Sunehag, G. Lever, C. De Witt, T. Lillicrap, D. Balduzzi, D. Reichert, V. Zambaldi, K. Tuyls, and T. Graepel, "Value-decomposition networks for cooperative multi-agent learning," in *Proceedings of the 16th International Conference on Autonomous Agents and MultiAgent Systems*, 2017, pp. 2085–2087.
- [38] T. Rashid, M. Samvelyan, C. De Witt, G. Farquhar, N. Nardelli, T. Rudner, and S. Whiteson, "Qmix: Monotonic value function factorization for deep multi-agent reinforcement learning," in *Proceedings of the 35th International Conference on Machine Learning*, 2018, pp. 4295–4304.
- [39] C. Yu, A. Velu, E. Vinitsky, J. Gao, Y. Wang, A. Bayen, and Y. Wu, "The surprising effectiveness of ppo in cooperative, multi-agent games," 2022. [Online]. Available: <https://arxiv.org/abs/2103.01955>
- [40] L. Lei, Y. Zhang, X. S. Shen, C. Lin, and Z. Zhong, "Performance analysis of device-to-device communications with dynamic interference using stochastic petri nets," *IEEE transactions on wireless communications*, vol. 12, no. 12, pp. 6121–6141, 2013.